Proton-Neutron Elastic Scattering on a Deuterium Target*

M. L. Marshak,† P. Schmueser,‡ J. L. Day,§ P. Kalbaci, A. D. Krisch, and J. K. Randolph‖
Harrison M. Randall Laboratory of Physics, University of Michigan, Ann Arbor, Michigan 48104

AND

G. J. Marmer and L. G. Ratner
Accelerator Division, Argonne National Laboratory, Argonne, Illinois 60439

(Received 9 July 1970)

We have tested the feasibility of measuring the ratio of proton-neutron to proton-proton elastic scattering using the second extracted proton beam of the Argonne ZGS and a liquid-deuterium target. The forward proton was detected by a 35-m-long spectrometer consisting of magnets and scintillation and Čerenkov counters. The recoil nucleon was detected by a steel-scintillator sandwich counter. The efficiency of this counter was measured using tagged neutrons in coincidence with the spectrometer and calculated using a Monte Carlo simulation of the nuclear cascade. A scintillation counter determined whether the recoil nucleon was charged or neutral. At a test point of $p_0=12.4$ GeV/c, $\theta^*=37°$, and $t=-2.2$ (GeV/c)^2, we found a pn-to-pp cross-section ratio of 1.05 ± 0.14. The pp cross section was $(d\sigma/d\Omega)_{\text{c.m.}}=5.8\pm0.6$ μb/sr, and the pn cross section was $(d\sigma/d\Omega)_{\text{c.m.}}=6.1\pm1$ μb/sr. The ratio of pp scattering from deuterium to pp scattering from hydrogen, corrected for geometrical effects, was 0.75 ± 0.09. We discuss the future of this technique for measuring pn cross sections and compare the results of the test with the predictions of the Glauber multiple-scattering formalism. We also plot available pn data as a function of $\beta_{\text{c.m.}}{}^2p_\perp{}^2$.

I. INTRODUCTION

The structure observed in proton-proton elastic scattering makes the isospin-related neutron-proton elastic scattering a process of considerable interest. For experimental reasons, the np elastic cross section has not been measured over nearly the same range of four-momentum transfers or with the same accuracy as the pp cross section. Experimental technique has allowed reliable measurements of proton-proton cross sections[1] as small as 10^{-36} cm^2/sr, corresponding to $t=-20$ (GeV/c)^2. It has not yet been possible to measure np cross sections[2] less than 10^{-30} cm^2/sr with comparable accuracy.

The difficulties encountered in previous np elastic scattering experiments are not very tractable since they arise from the characteristics of the incident neutron beam: (1) The intensity of a produced neutron beam is approximately a factor of a million less than the intensity of the primary proton beam. (2) The absolute intensity of the neutron beam cannot be easily measured; the observed differential cross sections are usually normalized to the optical point. This procedure results in a normalization uncertainty from the imprecise knowledge of the phase of the scattering amplitude. (3) The momentum spectrum of the neutron beam is broad, and can only be inferred from the analysis of scattering events; the necessity for reconstructing the incident momentum places tight demands on the resolution of detection of the outgoing particles.

In response to these deficiencies, we measured the pn elastic cross section using a proton beam and a deuterium target. This method solves all the problems of the neutron beam experiment since the proton beam has a high intensity, can be normalized by foil spallation techniques within 7%, and is monochromatic to ½%. However, the extraction of the free nucleon-nucleon cross section from the resultant raw data is complicated by several effects: (1) The Fermi momentum of the bound nucleons in the target deuteron smears the momentum and angular distributions of the scattered particles. Discrimination between elastic and inelastic events and double-arm detection of all elastic events become difficult. (2) Multiple-scattering or screening effects in the target deuteron affect the measured cross section. (3) Accurate quantitative results require the detection of the recoil nucleon with well-calibrated efficiency. A subsidiary problem is that the high background flux near an intense proton beam may swamp the large-volume counter required to detect a reasonable percentage of the recoil neutrons.

In order to correct for the first two effects, we simultaneously measured pp and pn elastic scattering from deuterium as well as pp scattering from hydrogen. The Fermi momentum effect is certainly identical for pp and pn scattering and drops out of a ratio of

$$R=\left(\frac{d\sigma}{d\Omega}\right)_{pn}\Big/\left(\frac{d\sigma}{d\Omega}\right)_{pp}. \tag{1}$$

* Work supported by the U. S. Atomic Energy Commission.
† Present address: School of Physics, University of Minnesota, Minneapolis, Minn. 55455.
‡ Present address: Department of Physics, University of Hamburg, 2000 Hamburg-50, West Germany.
§ Present address: Department of Physics, University of Pennsylvania, Philadelphia, Pa. 19104.
‖ Present address: Department of Physics, Haverford College, Haverford, Pa. 19041.
[1] G. Cocconi, V. T. Cocconi, A. D. Krisch, J. Orear, R. Rubinstein, D. B. Scarl, W. F. Baker, E. W. Jenkins, A. L. Read, and B. T. Ulrich, Phys. Rev. **138**, B165 (1965); J. V. Allaby, G. Bellettini, G. Cocconi, M. L. Good, A. N. Diddens, G. Matthiae, E. S. Sacharidis, A. Silverman, and A. M. Wetherall, Phys. Letters **25B**, 156 (1967).
[2] M. L. Perl, J. Cox, M. J. Longo, and M. N. Kreisler, Phys. Rev. D **1**, 1857 (1970); B. G. Gibbard, L. W. Jones, M. J. Longo, J. R. O'Fallon, J. Cox, M. L. Perl, W. T. Toner, and M. N. Kreisler, Phys. Rev. Letters **24**, 22 (1970); J. Engler, K. Horn, J. Konig, F. Monnig, P. Schludecker, H. Schopper, P. Sievers, H. Ullrich, and K. Runge, Phys. Letters **29B**, 321 (1969).

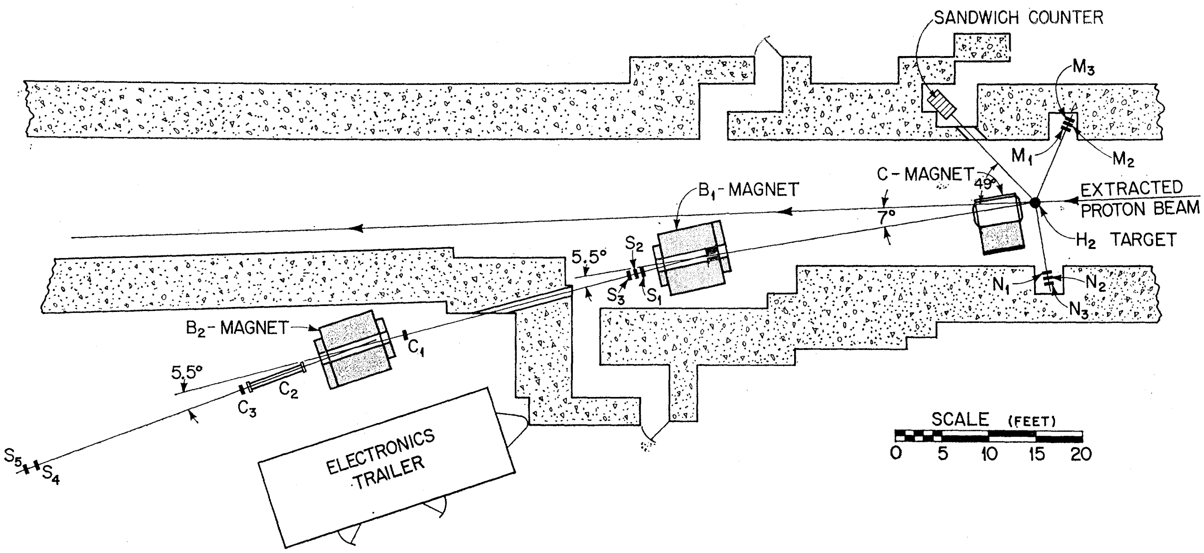

FIG. 1. Experimental layout. Forward proton is detected by the magnetic spectrometer and the recoil nucleon by the sandwich counter.

The detection of both the forward proton and the recoil nucleon in coincidence limits the types of multiple-scattering processes that can occur. The primary scattering must be at approximately the full momentum transfer and any scattering on the "spectator" nucleon must be at approximately zero momentum transfer in order to satisfy the kinematic requirements placed on the scattered particles. Thus only the scattering amplitudes at zero momentum transfer and the full momentum transfer are relevant. Since the forward pp and pn scattering amplitudes are approximately equal at high energies,[3] a consistency argument could indicate that the multiple-scattering correction also drops out of the cross-section ratio: Assume *a priori* that the multiple-scattering correction is isospin independent; if the resultant cross section is the same for pp and pn scattering, then the multiple-scattering correction should also be the same. In any event, if the multiple-scattering defect is a small percentage of the cross section, then any reasonable isotopic spin dependence should have a second-order effect on the cross-section ratio. Thus the free pn elastic cross section may be determined from the deuterium cross sections by the equation

$$\left(\frac{d\sigma}{d\Omega}\right)_{pn\ \text{free}}=\left[\left(\frac{d\sigma}{d\Omega}\right)_{pn\ \text{D}_2}\Big/\left(\frac{d\sigma}{d\Omega}\right)_{pp\ \text{D}_2}\right]\left(\frac{d\sigma}{d\Omega}\right)_{pp\ \text{free}}. \quad (2)$$

These ideas seem to indicate that the problems associated with the proton-deuterium method are more tractable than the difficulties encountered with the neutron beam technique. To determine their validity, we conducted a short feasibility test in the second extracted proton beam of the Argonne ZGS using essentially the same apparatus as in a previous experiment.[4] Because of the configuration of the apparatus available, we selected for measurement a test point at $p_0=12.4$ GeV/c and $\theta^*=37°$ or $t=-2.2$ (GeV/c)^2. The problem of neutron detection was approached using a steel-scintillator sandwich counter. A series of experimental measurements and Monte Carlo calculations determined the absolute detection efficiency of the counter over its entire sensitive area. The intensity of the incident proton beam was limited to 10^{10} protons/pulse so that the singles rate in the sandwich counter resulted in only a small correction for accidental coincidences.

II. EXPERIMENTAL METHOD

The physical layout of the experiment is shown in Fig. 1. The slow extracted proton beam impinged upon a liquid-deuterium target. The forward proton was identified and momentum-analyzed by a 35-m spectrometer composed of scintillation counters, bending magnets, and a threshold Čerenkov counter. The recoil nucleon passed through a scintillation counter, which determined whether it was charged, and was then detected in a steel-scintillator sandwich counter, shown in Fig. 2. The sandwich counter was made as large as possible so that the spectrometer basically defined the solid angle. Coincidence between the two arms was the indication of an elastic event. The number of protons incident on the target was measured by two monitor

[3] W. Galbraith, E. Jenkins, T. Kycia, B. Leontic, R. Phillips, and A. Read, Phys. Rev. 138, B913 (1965).

[4] J. L. Day, N. P. Johnson, A. D. Krisch, M. L. Marshak, J. K. Randolph, P. Schmueser, G. J. Marmer, and L. G. Ratner, Phys. Rev. Letters 23, 1055 (1969); J. L. Day, thesis, University of Michigan, 1970 (unpublished).

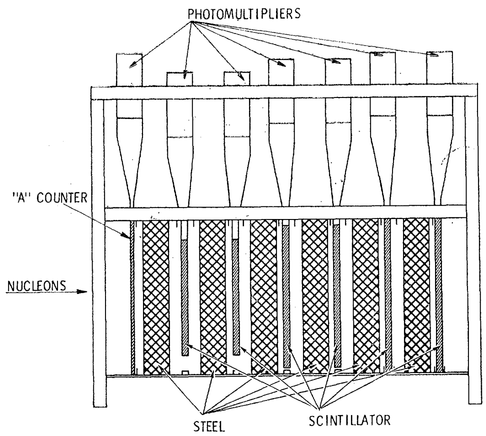

FIG. 2. Sideview of the steel-scintillator sandwich counter with the "12-in.-total—2-in.-between scintillators" steel configuration.

telescopes, which were calibrated by a radiochemical analysis of a gold foil exposed to the beam.

A. Proton Beam and Monitoring

A portion of the circulating proton beam was extracted from the ZGS main ring using the Piccioni energy-loss extraction system. After bending through four extraction magnets, the beam was focused by two sets of quadrupole doublets and was aimed down the experimental beam line by a 72-in. bending magnet. The upstream doublet consisted of two 36-in. quadrupoles and the downstream doublet was four 18-in. quadrupoles, divided into sets of two with the same focusing properties. The desired currents for both the quadrupoles and the bending magnets were computed by standard beam-design computer programs. The beam spot size at the target was optimized by replacing the liquid target with a $\frac{1}{4}$-in.-square copper target and searching for a maximum number of coincidences in the monitor telescopes as a function of the quadrupole currents.

The tuned beam at the target was $\frac{1}{2}$ in. full width at half-maximum (FWHM) both horizontally and vertically. The momentum was 12.4 GeV/c with an absolute uncertainty of $\pm\frac{1}{2}\%$. The angular divergence was less than 3 mrad FWHM, and the monochromaticity was better than $\pm\frac{1}{4}\%$. The beam intensity was 10^{10} protons per 550 msec spill. The repetition rate was one pulse every 3.3 sec.

The location and size of the proton beam were monitored visually after each ZGS pulse using two devices developed by the ZGS staff. A segmented wire ion chamber (SWIC)[5] located just upstream of the target displayed the extent of the beam, both horizontally and vertically, on an oscilloscope in the electronics trailer. The output of a beam ion position system (BIPS)[6] detector, placed approximately 15 m downstream of the target, was also located in the trailer. The long lever arm of the BIPS made it quite sensitive to small displacements in the beam position. Straying of the beam as indicated by the BIPS or SWIC was manually corrected by changing the current in the bending magnet in the beam line.

The two monitor telescopes, located just upstream of the target on each side of the tunnel, recorded coincidences in proportion to the number of protons incident on the target. The monitor counters were $\frac{1}{2}\times 1$-in. Pilot B scintillators; the axis of the three counters pointed to the target through a port in the target casing. The number of events in each telescope was multiplied by a fixed ratio to give each of the two monitor telescopes an approximately equal weight in the determination of the incident intensity. The monitors were normalized to the absolute beam intensity by measuring the characteristic activity of ^{149}Tb produced in a gold foil placed in the beam just upstream of the target during calibration runs. The uncertainty of ± 5 percent in the 1.05-mb spallation cross section for $^{197}\mathrm{Au}\rightarrow{}^{149}\mathrm{Tb}$ introduced a normalization error in the pp cross section but did not affect the pp elastic to pn elastic ratio.

B. Deuterium Target

The liquid-deuterium target, shown in Fig. 3, was a 3-in.-diam cylinder about a vertical axis. The target was self-refrigerating; an ADL cryostat produced liquid helium which cooled deuterium gas below its boiling point of 21°K. The amount of liquid in the target vessel was indicated by two thermistors, one located at the bottom and the other at the top.

The target flask was 0.003-in. H-film wrapped with several layers of 0.00025-in. aluminized Mylar superinsulation. A small hole cut in the Mylar allowed a visual check of the liquid level. The target vacuum casing was an aluminum cylinder with 0.322-in.-thick walls oriented about the beam axis with 0.005-in. H-film windows at each end. The forward proton exited through the downstream window, but the recoil nucleon passed through the aluminum vacuum vessel before reaching the sandwich counter. The ports facing the monitor counters were also covered with 0.005-in. H-film. The target-empty counting rate in the spectrometer alone was approximately 25% of the target-full rate, but the coincidence target-empty rate was only 1% of the full rate.

C. Spectrometer and Counters

The spectrometer which detected the forward proton was essentially identical to the one described in greater detail in Ref. 4. The two "B" magnets bent the proton through 5.5° each for momentum analysis. The "C"

[5] F. Hornstra, Jr., and J. R. Simanton, Nucl. Instr. Methods **68**, 138 (1969); J. R. Simanton, R. F. Margnardt, and F. Hornstra, Jr., *ibid.* **68**, 209 (1969).

[6] F. Hornstra, Jr., ZGS Report No. QR68-2, 1968 (unpublished).

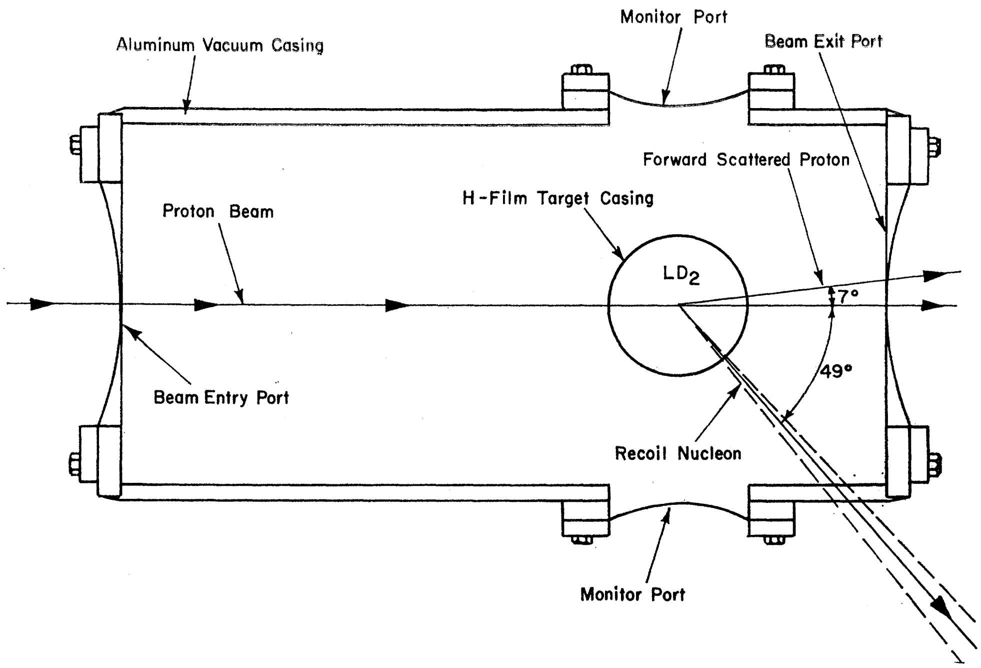

FIG. 3. Top view of the liquid-deuterium target and its vacuum casing. Dashed lines indicate the solid angle subtended by the sandwich counter.

magnet compensated for different particle-scattering angles by steering the desired protons into the spectrometer. For this experiment the forward proton was very close to the 7° central axis of the spectrometer, so the "C" magnet was operated at small or zero current. A spectrometer trigger required coincidence of all seven scintillation counters and an anticoincidence of a nitrogen-filled threshold Čerenkov counter.

The first three scintillation counters, located 60 in. downstream of the first "B" magnet, formed a triple coincidence $S_{123}=S_1S_2S_3$. The Čerenkov counter (C_2) was placed in anticoincidence ($C=C_1\bar{C}_2C_3$) with two nearby scintillation counters to eliminate pions or kaons. The two scintillation counters at the end of the spectrometer formed a double coincidence $S_{45}=S_4S_5$. The coupled momentum and horizontal scattering angle of the forward proton was defined by S_1 and S_5. S_5 alone defined the vertical acceptance. All other counters were overmatched.

The Pilot B scintillators were coupled to RCA 7746 photomultipliers by air light pipes for the three upstream counters and Lucite pipes for the rest. Using air light pipes and placing the Lucite pipes at various orientations reduced the coincidence rate due to Čerenkov radiation from particles passing through the light pipes. Light in the 72-in. Čerenkov counter was reflected by a 0.125-in. aluminized Lucite mirror through a light pipe into an RCA 8575 photomultiplier. This tube used a bialkalai photocathode to attain high quantum efficiency for low-level Čerenkov light. Voltages for all photomultipliers were determined by running standard plateau curves. The gas pressures for the Čerenkov counter were set after running pressure curves.

D. Sandwich Counter

The recoil nucleon was detected by the sandwich counter (T counter), which consisted of six 2-in. thicknesses of steel interspersed with six $\frac{1}{2}$-in. Pilot Y scintillation counters. The first two scintillators were 12 in. wide by 9 in. high; the next two were 14×11 in. and the last two were 15×12 in. The scintillators were optically connected to RCA 7746 photomultipliers by constant-area Lucite light pipes, to maximize light transmission. All the photomultiplier bases had a separate high-current supply for the last dynode and a Zener diode on the next-to-last dynode to eliminate voltage sag at high counting rates. A T-counter event occurred whenever there was at least one minimum-ionizing particle in any one of the six scintillation counters.

The photomultiplier voltages for the sandwich counter were set to equalize the output pulse heights for single minimum-ionizing particles. With all steel removed from the counter, high-voltage plateau curves were run on one counter in coincidence with two others or with the spectrometer. A spectrometer coincidence indicated that a minimum-ionizing recoil proton from a pp elastic scattering event in the target filled with hydrogen passed through the sandwich counter. This process was iterated until a consistent set of voltage settings emerged.

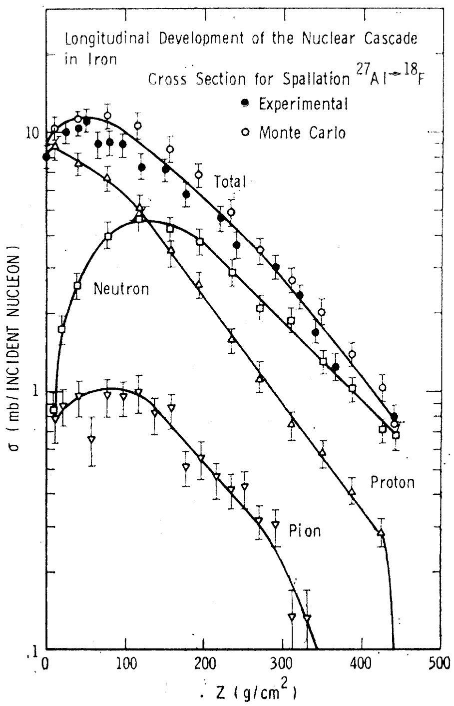

FIG. 4. Longitudinal development of the nuclear cascade from 1-GeV protons in a steel block. Errors shown are statistical only.

The sandwich counter was located 156 in. from the target at an angle of 49° from the beam. It was separated from the proton tunnel by an 18-in. steel wall with a hole cut to allow the recoil nucleons to reach the counter.

Directly in front of the sandwich counter, a $15\times12\times\frac{1}{4}$-in. scintillation counter was used to determine the charge of the recoil nucleon. Placing this A counter so close to the steel of the sandwich counter complicated the identification of the recoil nucleon. There was the possibility that a neutron could interact in the steel and backscatter a charged particle into the A counter, thus faking the signature of a proton. This ambiguity was corrected by the results of a Monte Carlo calculation, but uncertainties in the calculation limited the precision of the measurement of the pn to pp scattering ratio. A high-current supply and Zener diodes were also used for this counter to eliminate voltage sag at counting rates in excess of 1 MHz.

The relative efficiencies and solid angles for detecting protons and neutrons were calculated for the sandwich counter using a Monte Carlo simulation of the nuclear cascade, which is described in detail in Ref. 7. The counter detected a proton if it or its reaction products passed through 2 in. of steel and reached the first scintillator. It detected a neutron only by production of charged secondaries which passed through one of the scintillation counters. The detection of neutrons near the edges of the counter was also hampered by the possibility that all charged reaction products might scatter outside the sensitive volume.

The Monte Carlo simulation followed the general method of earlier calculations for shielding purposes.[8] As the incident nucleon and its reaction products passed through the counter, they were subject to elastic and inelastic scattering in accordance with the probabilities given by Ranft.[8] The momentum and angular distributions for the scattered particles after an inelastic collision were computed according to commonly used fits to particle production spectra.[8] The types of particles produced were determined by experimental multiplicities for this momentum region[9] and the number of particles produced was set by the requirement of conservation of energy. Since most quasi-elastic scattering involves a small momentum transfer, the recoil particle for this process was ignored. Ionization and multiple Coulomb scattering were calculated for charged particles. Neutral-pion decay into two γ rays was considered and the probability of γ conversion was interpolated from the results of Monte Carlo calculations of

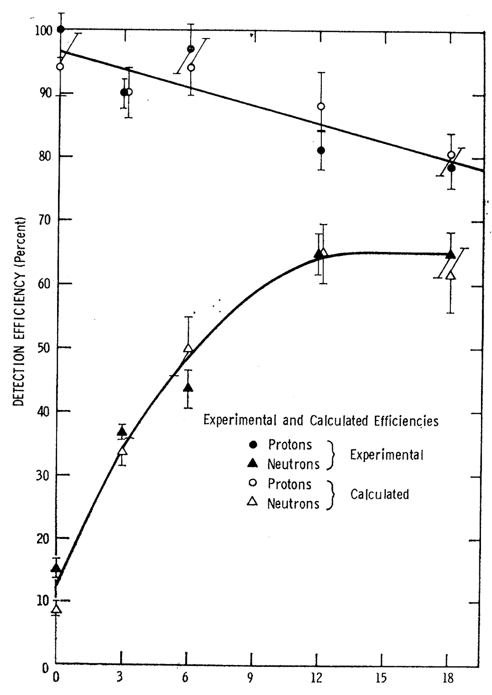

FIG. 5. Comparison of the experimental and calculated counting rates for the sandwich counter with different steel configurations. Recoil-nucleon and backscattering effects are included in the calculated rates.

[7] M. L. Marshak and P. Schmueser, Nucl. Instr. Methods **85** (to be published, 1970).

[8] J. Ranft, Nucl. Instr. Methods **48**, 133 (1967); T. W. Armstrong and R. G. Alsmiller, Jr., Nucl. Sci. Eng. **33**, 291 (1968).

[9] V. S. Barashenkov, V. M. Maltsev, I. Patera, and V. D. Toneev, Fortschr. Physik **14**, 357 (1966).

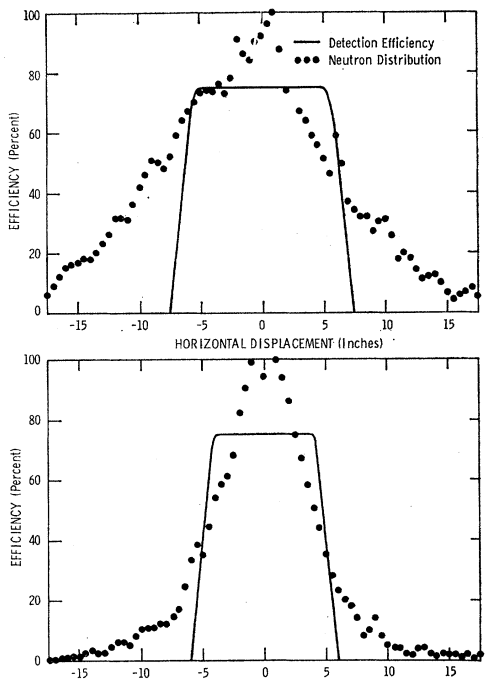

FIG. 6. Calculated sandwich-counter detection efficiency for neutrons and the recoil-neutron distribution along the horizontal and vertical axes of the counter.

the electromagnetic cascade.[10] For simplicity, charged-pion decay was ignored.

The reliability of the Monte Carlo model was determined by two different methods. The validity of the assumptions concerning the nuclear cascade were tested by calculating the ^{18}F activity induced by 1-GeV protons in thin aluminum foils interspersed in a block of steel. The calculated activities were compared with measurements made by Shen[11] for a similar situation as shown in Fig. 4. The second method, which tested both the nuclear and electromagnetic portions of the model, involved calculation of the apparent proton and neutron counting rates for seven different steel configurations of the sandwich counter, including no steel. The coincidence counting rate for both *pn* and *pp* events was also experimentally measured for the same steel configurations. The number of events in the spectrometer, which detected the sum of *pn* and *pp* scattering independently of the sandwich counter, was used as a monitor for these runs. The coincidence rates displayed the same dependence on steel thickness as the calculated proton and neutron efficiencies, as shown in Fig. 5. By adjusting the normalization of the experimental curves to fit the calculated curves, the remaining parameter—the ratio of *pn* to *pp* scattering—was fixed. The χ^2 confidence level for this fit was larger than 40%.[12]

The calculated neutron detection efficiency was $(75\pm6)\%$ at the center of the sandwich counter and dropped toward the edges as shown in Fig. 6. The calculated central detection efficiency for protons was $(98\pm1)\%$. The proton efficiency profile is shown in Fig. 7.

The assessment of the given errors in the Monte Carlo calculation followed from a detailed analysis of the various reasons for counter inefficiency. The error in determining that 25% of the incident neutrons were not detected could be divided into two parts. Approximately 15% of the neutrons passed through the counter without interacting; this number was dependent only on the inelastic cross section. Knowledge of that cross section to 10% implied only a 3% error in the detection efficiency. This left 10% of the incident neutrons which interacted but were not detected because of production of neutrals, absorption of charged secondaries, or scattering of secondaries outside the sensitive volume. Assumption of a somewhat arbitrary 50% error in the calculation of this process implied a 5% error in the over-all efficiency. Considering these errors in quadrature resulted in the central detection efficiency uncertainty of 6%.

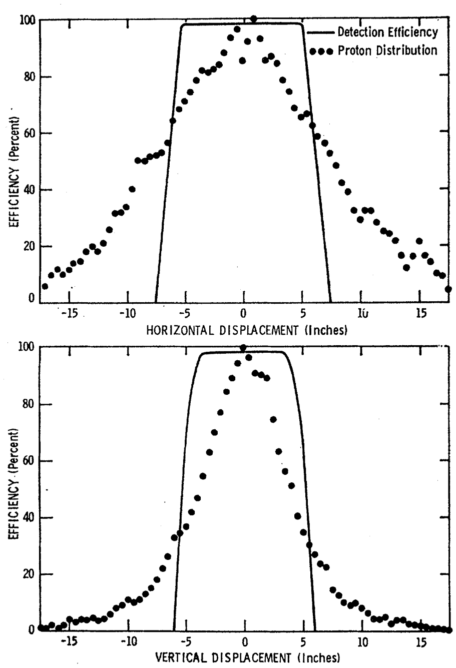

FIG. 7. Calculated sandwich-counter detection efficiency for protons and the recoil-proton distribution along the horizontal and vertical axes of the counter.

[10] D. F. Crawford and H. Messel, Nucl. Phys. 61, 145 (1965).

[11] S. P. Shen, BNL Report No. BNL-8721, 1964 (unpublished).

[12] In calculating the χ^2, the no-steel point for neutrons was ignored. This procedure was reasonable since the predictions of a model based on neutron-steel interactions could not be relevant when only neutron-scintillator interactions could occur.

Two other factors were involved in calculating the correction to the data for sandwich-counter efficiency. The detection function for the counter was weighted by the distribution of recoil nucleons across the face of the counter. This nonuniform distribution was influenced by the Fermi momentum of the target deuteron as well as by the angular divergence and momentum dispersion of the beam, the phase-space bite of the spectrometer, and the finite size of the target. The calculated horizontal and vertical distributions are shown in Figs. 6 and 7 for the maximum counting-rate point. The asymmetry in the horizontal distributions was due to not setting at the exact maximum of the quasi-elastic peak, which resulted from the $\pm\frac{1}{2}\%$ uncertainty in the incident momentum. Scanning across the quasi-elastic peak minimized any uncertainty from this effect in the final cross-section ratio.

The other correction involved the possibility of a charged secondary from an incident neutron backscattering into the A counter. The Monte Carlo simulation calculated that $(11.6\pm4)\%$ of the recoil neutrons were detected as protons because of backscattering. Approximately half the backscattered charged particles were low-energy pions; the remainder were mostly electrons from a converted γ along with a few protons. The 4% uncertainty includes an estimation of systematic effects, as well as Monte Carlo statistical errors.

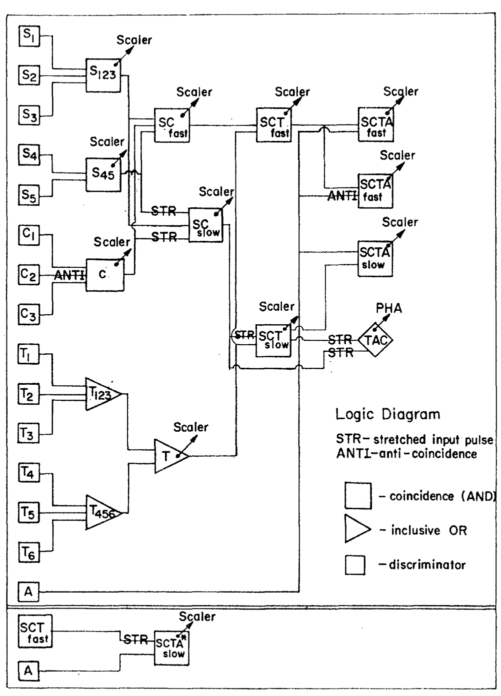

FIG. 8. Block diagram of the logic for the various slow and fast coincidences and the time-of-flight spectrum.

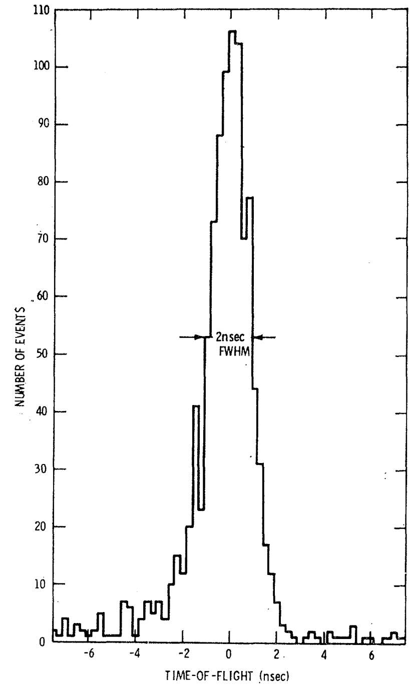

FIG. 9. Typical two-arm time-of-flight spectrum with a width of 2 nsec FWHM.

E. Electronics

Signals from the photomultipliers were logically analyzed by Chronetics 100-Mhz circuitry. Compatible TSI scalers displayed the output of the logic system. A TMC 400-channel pulse-height analyzer accumulated and displayed the time-of-flight spectrum between the two detector arms.

The trigger indicating that a proton of the proper momentum passed through the spectrometer was the triple coincidence $SC_{\text{fast}}=S_{123}S_{45}C$, where $C=C_1\bar{C}_2C_3$. As shown in Fig. 8, this signal and the logical OR output of the sandwich counter formed a twofold coincidence $SCT_{\text{fast}}=SC_{\text{fast}}T$, which indicated an elastic scattering event. To separate pp elastic from pn elastic events, the SCT_{fast} signal formed both a twofold coincidence and a twofold anticoincidence with the A counter. These outputs were separately scaled as $SCTA_{\text{fast}}$ for pp events and $SCT\bar{A}_{\text{fast}}$ for pn events.

The high singles rates in both the sandwich and A counters, typically of order 1 MHz, necessitated the formation of additional coincidences to permit correction for accidentals. A second coincidence, with a resolving time much longer than the first, allowed extrapolation of the coincidence rate to zero resolving time. The outputs of S_{123}, S_{45}, and C were stretched by separate discriminators and formed another triple coincidence SC_{slow} with a resolving time of 30 nsec as opposed to 5 nsec for SC_{fast}. The extrapolation method calculated that the number of accidentals in SC_{fast} was $\frac{1}{5}(SC_{\text{slow}}-SC_{\text{fast}})$. Similarly, the SC_{slow} output was stretched and formed a twofold coincidence with T, SCT_{slow} with a resolving time of 60 nsec compared with 7 nsec for the fast coincidence. The SCT_{slow} output formed a fast coincidence with A; this coincidence was separately scaled as $SCTA_{slow}$. For some data runs another system of slow coincidences was used. SC_{slow} and SCT_{slow} were formed as before, but the output of SCT_{fast} was stretched in a discriminator and formed a twofold coincidence with A with a resolving time of 50 nsec which was scaled as $SCTA^*_{slow}$. The resolving times for the $SCTA_{fast}$ and $SCT\bar{A}_{fast}$ coincidences were 10 and 5.5 nsec, respectively.

The true number of triggers of the type $SCTA$ and $SCT\bar{A}$ was determined by solving a set of five simultaneous linear equations involving SCT_{fast}, SCT_{slow}, $SCTA_{fast}$, $SCTA_{slow}$, and $SCT\bar{A}_{fast}$. Three types of accidental coincidences were considered significant and included in the calculation—an accidental between arms associated with an A count, an accidental between arms not associated with an A count, and a true coincidence between arms associated with an accidental A count. The calculation of the five quantities (three types of accidentals and the number of protons and neutrons) from five observables resulted in a no-constraint fit. For the second electronics arrangement, which formed $SCTA^*_{slow}$, the 5×5 accidentals correction matrix was singular and consideration of the two-arm accidental associated with an A count was dropped, yielding a nonsingular 4×4 matrix. This procedure introduced only a small error since this type of accidental was consistently the most infrequent in those data runs for which it could be calculated.

To check the accuracy of the whole system of slow and fast coincidences, a time-of-flight spectrum between the two arms was accumulated. The timing overlap between two stretched pulses from the SC_{slow} and the SCT_{slow} coincidences was converted to a pulse height by a time-to-amplitude converter (TAC). The TAC output was analyzed by a pulse-height analyzer and printed out at the end of each data run as a spectrum with a width of $\sim$2 nsec FWHM. A typical spectrum with a resolution of approximately $\frac{1}{4}$ nsec per channel is shown in Fig. 9.

As indicated in Table I, the accidentals correction was 3% for pp events from hydrogen and 9% for pp events from deuterium. There was no net accidentals correction for pn events from deuterium, although the uncertainty in the two offsetting corrections from different types of accidentals resulted in a 4% total uncertainty in that result. These two types of accidentals each amounted to approximately 10% of the total number of pn events.

III. RESULTS

A. Corrections and Experimental Errors

The major systematic errors in the experiment arose from an uncertainty in the magnitude of corrections to the raw experimental data. Corrections were made for nuclear absorption, multiple Coulomb scattering, sandwich-counter efficiency, backscattering in the sandwich counter, discriminator deadtime, accidental coincidences, and target-empty counting rate. Data points outside the quasi-elastic peak were used to extrapolate

TABLE I. Errors and corrections.

Type	pp events (hydrogen)		pp events (deuterium)		pn events (deuterium)	
	Correction	Error (%)	Correction	Error (%)	Correction	Error (%)
Accidental coincidences	0.97	1	0.91	3	1.00	4
Discriminator deadtime	1.02	1	1.02	1	0.98	1
Target-empty events	0.99	0	0.99	0	0.99	0
Inelastic events	0.975	1	0.975	1	0.92	3
Absorption:						
Spectrometer	1.15	3				
Recoil particle	1.04	1				
Sandwich counter:						
Backscattering			0.92	3	1.12	4
Detection efficiency	1.02	1	1.02	1	1.33	6
Geometrical efficiency	1.24	5				
Multiple Coulomb scattering (recoil proton)	1.02	1	1.02	1		
Monte Carlo phase-space calculation (statistical)		3		3		4
Experimental statistics		4.5		3.2		3.9
Monitoring of incident intensity:						
Spallation cross section		5				
Relative (point-to-point)		2		2[a]		

Total: pp cross-section from hydrogen: 10%; pn/pp ratio (deuterium): 13%; pp (hydrogen)/pp(deuterium) ratio: 8%; pn cross section: 16%.

[a] Contributes to $pp(H_2)/pp(D_2)$ ratio but not to pn/pp ratio.

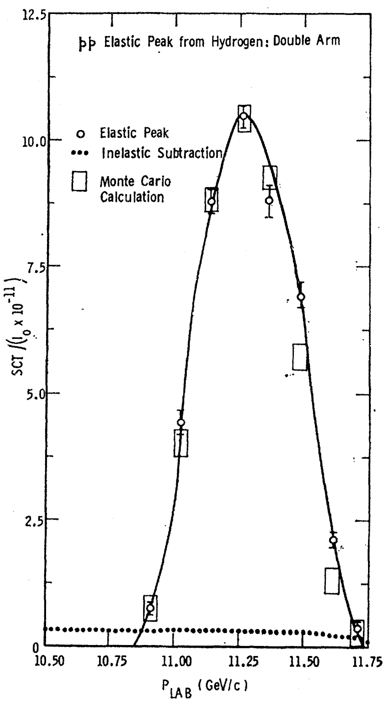

FIG. 10. pp elastic scattering peak from hydrogen using two-arm coincidence data.

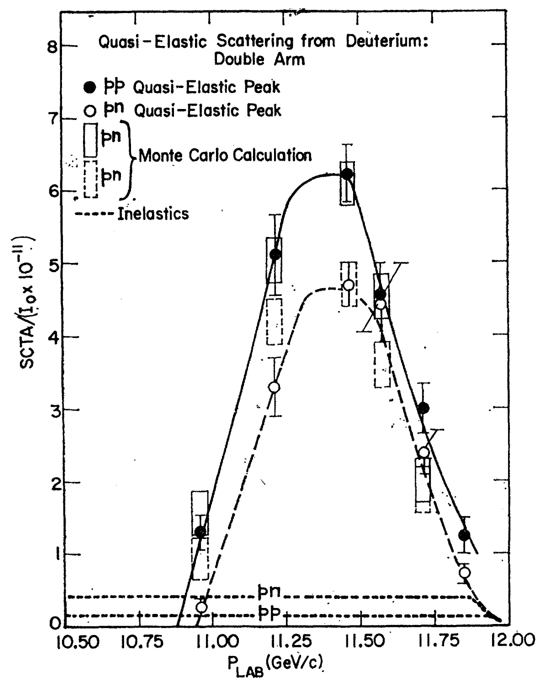

FIG. 11. pp and pn quasi-elastic peaks from deuterium using two-arm coincidence data.

a uniform inelastic background subtraction under the peak. As shown in Table I, the subtraction was 2.5% of the peak for pp scattering and 8% for pn scattering. The different subtractions indicated the possibility of additional "noise" in the pn signal because one less coincidence was required ($SCT\bar{A}$ for pn instead of $SCTA$ for pp). The size of the subtraction was consistent with Monte Carlo studies, which showed that only $N^*(1238)$ production could result in a large background. Since the $N^*(1238)$ cross section falls quickly with momentum transfer,[13] for the point measured the background was small. The phase space for each data point in the scan across the quasi-elastic peak was also calculated by a Monte Carlo program which considered target spot size, angular divergence, and chromatic dispersion. The agreement shown in Figs. 10 and 11 between the shape of the experimental quasi-elastic peak and the phase-space calculation of the shape confirms the reasonableness of the inelastics subtraction.

Only some of the corrections and their associated systematic errors were applicable to any given datum from the experiment. Nuclear absorption and multiple Coulomb scattering in the spectrometer, for example, affected the absolute pp cross section but not the pn to pp cross-section ratio. By far the greatest part of the error in that ratio resulted from uncertainty in the determination of the detection efficiency of the sandwich counter. Table I lists the corrections applicable to each of the determined experimental quantities, the amount of the correction, and an estimate of the associated systematic error.

The corrections for nuclear absorption were calculated by a Monte Carlo program using appropriate interaction lengths[14] and the same secondary-particle spectra as were used for the sandwich-counter calibration program. The same Monte Carlo program also determined the multiple-Coulomb-scattering correction using a Gaussian distribution for the scattering angle. The detailed sandwich-counter efficiency profile was folded together with a Monte Carlo calculation of the distribution of recoil nucleons over the face of the counter to determine the correction for sandwich-counter inefficiency. The discriminator dead time was taken as twice the duty factor of 1% to compensate for rf structure in the beam. Where comparison was possible, the accidentals subtraction generated by the system of fast and slow coincidences agreed to well within experimental errors with the results of the time-of-flight spectrum. The target-empty subtraction was determined by taking otherwise identical data runs with neither hydrogen nor deuterium in the target flask.

B. Proton-Proton Scattering

Proton-proton elastic scattering was measured for the test point of $p_0 = 12.4$ GeV/c, $\theta^* = 37°$ using both hy-

[13] C. M. Ankenbrandt, A. R. Clark, Bruce Cork, T. Elioff, L. T. Kerth, and W. A. Wenzel, Phys. Rev. **170**, 1223 (1968).

[14] N. Barash-Schmidt, A. Barbaro-Galtieri, L. R. Price, M. Roos, A. H. Rosenfeld, P. Söding, C. G. Wohl, M. Roos, and G. Conforto, Rev. Mod. Phys. **41**, 109 (1969).

drogen and deuterium targets. Measuring with both targets determined the free pp elastic cross section—a parameter required in Eq. (2)—and permitted a large-angle check of the Glauber formalism for multiple scattering.[15] The difference between the elastic pp cross section from hydrogen and the quasi-elastic pp cross section from deuterium included the effect of geometrical inefficiency due to the Fermi momentum as well as the multiple-scattering defect. To test the Glauber formalism it was necessary to extract the multiple-scattering contribution by calculating the effect of geometrical inefficiency. This calculation depended somewhat on the form used for the deuteron wave function. This dependence was not large because only Fermi momenta $\gtrsim 150$ MeV/c were relevant to the calculation. Over this range in momentum space, most proposed wave functions are approximately equal.[16] For the results given here, the Moravcsik fit to the wave function of the Hulthén type[16] was used in the Monte Carlo calculation of the geometrical inefficiency.

The observed free pp cross section was calculated according to

$$\frac{d\sigma}{d\Omega}=\left(\frac{1}{N_0\rho t I_0 \Delta\Omega}\right)(\text{corrected no. of events}), \qquad (3)$$

where N_0 is Avogadro's number, ρ is the density of liquid hydrogen (0.07 g/cm^3), t is the length of the target (2.9 in.), I_0 is the incident beam intensity, and $\Delta\Omega$ is the solid angle in the center-of-mass system. The measured pp center-of-mass cross section was

$$(d\sigma/d\Omega)_{\text{c.m.}}=5.8\pm0.6\ \mu\text{b/sr},^{17}$$

including a 5.4% normalization error, a 4.5% statistical error, and a 7.2% systematic error. The over-all cross-section ratio for pp scattering from deuterium to pp scattering from hydrogen was

$$\text{deuterium/hydrogen}=0.39\pm0.03. \qquad (4)$$

After including the results of the calculation of geometrical inefficiency, the ratio due to multiple-scattering effects alone was

$$\text{deuterium/hydrogen}=0.75\pm0.09. \qquad (5)$$

The error does not include any uncertainty resultant from the use of an approximation for the deuteron wave function in the geometrical-inefficiency calculation.

[15] V. Franco and R. J. Glauber, Phys. Rev. **142**, 1195 (1966); J. V. Allaby, A. N. Diddens, R. J. Glauber, A. Klovning, O. Kofoed-Hansen, E. J. Sacharidis, K. Schlüpmann, A. M. Thorndike, and A. M. Wetherall, Phys. Letters **30B**, 549 (1969).

[16] M. J. Moravcsik, Nucl. Phys. **7**, 113 (1958).

[17] This pp cross section agrees well with nearby measurements done at CERN. See J. V. Allaby, A. N. Diddens, A. Klovning, E. Lillethun, E. J. Sacharidis, K. Schlüpmann, and A. M. Wetherell, Phys. Letters **27B**, 49 (1968).

C. Proton-Neutron Scattering

By the arguments already given, the determination of the pn elastic cross section is independent of geometrical effects, except for sandwich-counter efficiency, and of multiple-scattering effects if $R\approx 1$. The measured ratio of pn scattering to pp scattering, corrected for all experimental effects, was

$$R=\left(\frac{d\sigma}{d\Omega}\right)_{pn}\bigg/\left(\frac{d\sigma}{d\Omega}\right)_{pp}=1.05\pm0.14. \qquad (6)$$

The equality of the pn and pp cross sections makes the consistency argument of Sec. I applicable[18]; the measured pn elastic cross section at the test point of $p_0=12.4$ GeV/c and $t=-2.2$ (GeV/c)^2 was then

$$(d\sigma/d\Omega)_{\text{c.m.}}=6.1\pm1\ \mu\text{b/sr}$$

or

$$d\sigma/dt=3.5\pm0.6\ \mu\text{b}/(\text{GeV}/c)^2.$$

IV. DISCUSSION

A. Neutron-Proton Elastic Scattering

The neutron-proton elastic differential cross section is plotted in Fig. 12 as a function of $\beta_{\text{c.m.}}{}^2 p_\perp{}^2$, the variable used by Krisch for an energy-independent plot of all high-energy pp elastic scattering data.[19] All of the available large-momentum-transfer data and a representative sample of the small-momentum-transfer data are included in the plot.[2] This variable seems to account for the shrinkage of the diffraction peak for np scattering as well as it does for pp scattering, although the large experimental-error bars inhibit a highly constrained fit to a straight line. The slope of the diffraction peak is slightly, but significantly, less steep than the slope of the pp diffraction peak: 8.5 (GeV/c)$^{-2}$ for np scattering and 10 (GeV/c)$^{-2}$ for pp scattering. In the context of a Lorentz-contracted optical model, the outer radius of the np interaction is then 0.81 F compared with 0.88 F for the pp interaction.[20] Similar to the pp data, the np cross section exhibits a "break" at $\beta_{\text{c.m.}}{}^2 p_\perp{}^2=0.7$ (GeV/c)^2, although experimental errors prevent a quantitative determination of the slope for the region outside the diffraction peak. There are

[18] We have investigated the effect on the uncertainties in the pn cross-section measurement if Eq. (2) were not the proper treatment of the multiple scattering. If we assume that the multiple-scattering correction is additive, rather than multiplicative, but still identical for pp and pn, the ratio R becomes 1.04 ± 0.17. If we assume an additive correction, unequal in the same proportion as the cross sections from deuterium for pp and pn, then $R=1.09\pm0.23$. There are other possibilities for the multiple-scattering correction which change R even more, but we consider Eq. (2) the most probable relationship and these other two possibilities the next most probable. Including these possibilities could increase the uncertainties in the pn cross-section measurement from 16 to 21%.

[19] A. D. Krisch, Phys. Rev. Letters **19**, 1149 (1967).

[20] A. D. Krisch, in *Lectures in Theoretical Physics*, edited by W. E. Brittin *et al.* (University of Colorado Press, Boulder, Colo., 1966), Vol. IX.

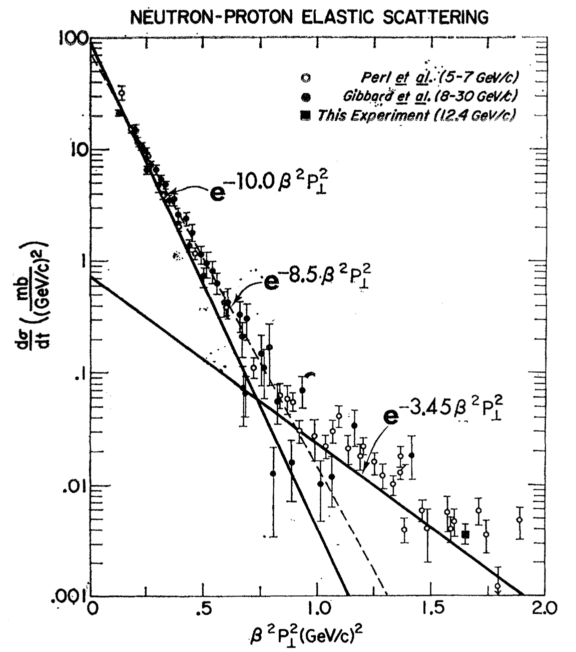

FIG. 12. A plot of np elastic cross sections as a function of $\beta_{\text{c.m.}}{}^2 p_\perp{}^2$. The solid line is the Krisch fit to the "fundamental" pp cross section $d\sigma^\dagger/dt$.

presently no data at large enough momentum transfer to indicate whether the np cross section also follows the second "break" observed in the pp cross section at $\beta_{\text{c.m.}}{}^2 p_\perp{}^2 = 2.8$ $(\text{GeV}/c)^2$.

The np system is free from particle-identity effects which complicate pp scattering near 90° c.m. The data point from this feasibility test and the results of previous experiments indicate that the np and pp cross sections are approximately equal in the small-momentum-transfer region. Recent results[2] for incident momenta from 3 to 6 GeV/c indicate that the cross-section ratio at 90° c.m. is given by

$$(np/pp)|_{90^\circ} = 0.63 \pm 0.09. \tag{7}$$

This ratio is graphically illustrated in Fig. 12 where the solid line represents the Krisch fit to $d\sigma^\dagger/dt$, which is presumably the "fundamental" pp cross section independent of particle-identity effects.[19] If this model is correct and if the "fundamental" cross section is independent of nucleon type, then the np data should lie along the line. Because of particle-identity effects, the experimental pp cross section at 90° c.m. is a factor of 2 above the line, if the interaction is spin independent.

B. Multiple Scattering

Application of the Glauber formalism to the test point measured in this experiment is complicated by both the small-angle and closure approximations in the model. Closure is assumed in the derivation to permit summation over all allowed proton-neutron final states. The geometry of this experiment does not permit detection of a complete set of proton-neutron final states, so the closure approximation is invalid. It is difficult to determine the error introduced into the final results by these approximations. The Glauber prediction[15] for the ratio of pp scattering from deuterium to pp scattering from hydrogen is

$$\text{deuterium/hydrogen} = 0.85, \tag{8}$$

using a Gaussian deuteron form factor and Krisch's form for the nucleon-nucleon scattering amplitudes.[19] The measured ratio is 0.75 ± 0.09, indicating no significant disagreement.

The Glauber model, even if it is not particularly applicable, indicates that both the multiple-scattering defect and the amount of quasi-elastic scattering relative to two-body elastic scattering increase with increasing momentum transfer. The experimental results confirm this prediction qualitatively and indicate a perhaps greater magnitude than the theory for the multiple-scattering defect. Without a detailed, applicable model it is difficult to determine the complete angular distribution for the multiple-scattering defect from the two experimental points at $\theta^* = 0°$ and 37°. The only other available data show the same trend but are at 1.69 GeV/c incident proton momentum.[21]

C. Deuterium Target Technique

The errors associated with the cross section measured in this experiment are somewhat smaller than the errors for the neutron beam technique cross sections of approximately the same magnitude. This comparison indicates that despite some systematic uncertainties, the proton-beam–deuterium-target method promises substantially improved measurements of the np elastic cross section, especially at large transverse momentum.

The errors in this feasibility test can probably be reduced significantly. The largest single uncertainty in the pn/pp ratio is associated with backscattering in the sandwich counter. This correction can be eliminated entirely by moving the A counter far enough from the sandwich counter so that timing discrimination can eliminate false triggers. More extensive experimental measurements of the efficiency of the sandwich counter for neutron detection could eliminate some of the uncertainty which results from imprecise knowledge of the detection efficiency. Time-of-flight spectra on all coincidences would reduce the errors due to accidental coincidences. The use of a hodoscope to provide better resolution of the elastic peak would allow a more careful subtraction of the inelastic background. All these improvements are well-known experimental techniques although they necessarily increase the complexity and cost of the experiment. To measure an angular distribu-

[21] A. T. Murray, L. Riddiford, G. H. Grayer, T. W. Jones, and Y. Tanimura, Nuovo Cimento 49A, 261 (1967).

tion, an additional complication is the necessity for mounting the sandwich counter and its associated shielding on a movable platform. Implementing all these improvements would reduce the experimental error in the *pn*/*pp* ratio from 15% to less than 7%.

A post-experiment review of the three problems anticipated with the deuterium method indicates that they are all relatively tractable. The smearing effect of the Fermi momentum is unfortunate because it reduces the counting rate, but it can be reasonably well calculated. Indeed as the scattering angle increases, the laboratory momentum of the recoil nucleon increases. Since the angular smearing depends approximately on the ratio $p_{\text{Fermi}}/p_{\text{recoil}}$, the smearing and thus the inefficiency become smaller. The loosening of the kinematic constraints on elastic scattering because of the Fermi momentum does not result in an unmanageable inelastic background.

The consistency argument provides a reasonable approach to the problem of multiple scattering in the deuteron if the *np* and *pp* cross sections are approximately equal. That the cross sections are not equal over the entire angular range seems likely from both experimental data and theoretical considerations. At 90° c.m., the Pauli principle forces inequality unless the nucleon-nucleon scattering amplitudes have a very particular helicity structure. If $R \neq 1$, the effects of multiple scattering at large momentum transfers are not determinable from present theoretical models. Fortunately for the proton-beam–deuterium-target method, the cross-section ratio seems to differ from unity only near 90° c.m. For large-angle scattering, the difference between the quasi-elastic *pp* cross section and the elastic *pp* cross section is smaller than at small angles where elastic *pd* scattering dominates. The smaller the difference between the quasi-elastic and elastic cross sections and the smaller the difference from unity of the *pn* to *pp* cross-section ratio, the smaller the uncertainty in the final result attributable to multiple-scattering effects.

The sandwich counter seems a reasonable solution for neutron detection. To allow higher beam intensities which will permit measurements of considerably smaller cross sections, we have investigated by Monte Carlo methods alternate triggering schemes for the sandwich counter which would considerably reduce the counter singles rates. Such schemes seem feasible particularly for the higher-momentum recoil neutrons which are produced from interactions at larger scattering angles or higher incident momenta. One possibility would be to require two adjacent scintillators to count instead of any one scintillator. This trigger would place a range requirement on the charged secondaries and therefore set a low-energy cutoff on the particles detected.

The most interesting experiment would be to investigate the ratio of *pn* to *pp* scattering over the full angular range. The presently poor understanding of the multiple-scattering correction at 90° c.m. would partially impair the credibility of some of the results, but since there is no large angle data above 7 GeV/*c*, all of the data would be useful. There is the additional prospect that this data would help unravel the structure of multiple-scattering processes at large momentum transfers. With a higher-energy beam, the *pd* method could determine the existence of a second "break" in the *np* scattering cross section, avoiding completely the 90° c.m. problem. In any event, direct measurement of the *pn* to *pp* scattering ratio should reveal considerable information about the spin and isospin structure of nucleon-nucleon scattering.

ACKNOWLEDGMENTS

We express our appreciation to the entire ZGS staff for their assistance and encouragement in performing this experiment. We particularly thank Dr. W. F. Baker for several helpful discussions and for aid in the preliminary stages of the experiment. We also thank N. P. Johnson for participation in the preparation of the experimental apparatus.